CRYSTAL GROWTH & DESIGN

Article

pubs.acs.org/crystal

Layered Dinitrostilbene-Based Molecular Solids with Tunable Micro/Nanostructures and the Reversible Fluorescent Response to Explosives

Dongpeng Yan,* Yanjun Lin, Qingyun Meng, Minjun Zhao, and Min Wei

State Key Laboratory of Chemical Resource Engineering, Beijing University of Chemical Technology, Beijing 100029, P. R. China

Supporting Information

ABSTRACT: The ability to modulate and control the fluorescence properties of molecular solids at the micro/nanoscale is important to develop high-performance optoelectronic materials and sensors. Here we report the tunable one-photon and two-photon fluorescence as well as micro/nanostructures of dinitrostilbene-based (DNS) chromophore by the formation of layered multicomponent crystals with guanidinium cation (GD) through hydrogen-bonding assembly. The as-prepared GD_2DNS bulk crystal shows a red-shift emission as well as enhanced photoluminescence quantum yield and fluorescence lifetime compared with those of the Na_2DNS sample, which is related to the structural transfer of DNS from staggered arrangement to parallel fashion within the crystal. Periodic density functional theoretical calculations further show that the introduction of different cationic units can modify the frontier orbital distribution and electronic structure of DNS anions within the multicomponent crystals. Moreover, one-dimensional GD_2DNS nanobelts with well-aligned orientation can be further obtained by a combined ultrasound and coprecipitation method. The GD_2DNS nanobelts undergo a blue-shift fluorescence compared with its bulk crystal, and exhibit alternated photoresponse (such as emission wavelength and intensity) upon interaction with different nitroaromatic explosives (trinitrotoluene, picric acid and m-dinitrobenzen). Therefore, this work gives a facile bottom-up self-assembly rout to prepare organic multicomponent materials with tunable fluorescence properties and micro/nanostructures, which can be potentially used as luminescence detector for nitroaromatic explosives.

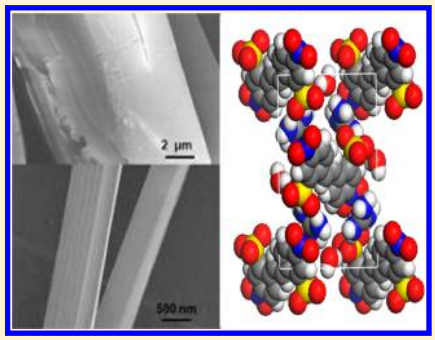

1. INTRODUCTION

Organic photoactive materials have received considerable attention due to their potential applications in fields of dye lasers,[1] light-emitting diodes,[2] and fluorescent sensors.[3] From the perspectives of both fundamental research and practical applications, the regulation of the solid-state luminescent properties of an organic material is important to realize multicolor displays and tunable light-emitting device.[4] To date, the key strategy to tune the fluorescence of a compound is to alter its molecular arrangement and packing mode.[5] In this case, intermolecular interactions within the organic solid can be further modified.[6] Specifically for small organic chromophores, the formation of polymorphisms[7] and multicomponent crystals[8] can result in the changeable luminescence. Compared with the polymorphisms, the multicomponent crystals (such as cocrystals[9] and salts[10]) present more predictability, which can be designed by appropriate selection and design of building blocks and the interaction types (such as hydrogen-[11] and halogen-bonding[12]) within the crystal based on the supramolecular assembly principle.[13] Several studies have shown that the construction of multicomponent crystals can result in the fine-tuning of supramolecular structures and thus further tailor the photo-related properties of organic solid state materials.[14]

Recently, a great deal of effort has been paid to the synthesis of pure organic chromophores with variable morphologies at the micro/nanometer level.[15] The as-obtained organic micro/nanomaterials can present alternated photophysical properties compared with those of the bulk, due to the size-dependent effect.[16] Moreover, low-dimensional organic micro/nanostructures also endowed great opportunities to develop miniaturized optoelectronic devices, such as the optical waveguide and fiber materials.[17] However, the investigation on the optical properties of organic multicomponent micro/nanomaterials is still in an early stage, and examples are rather few.[18] Such self-assembled systems organized from two or more organic units can result in unique photophysical behaviors,[19] which also supply an effective way to tune the compositions within the micro/nanostructures and thus extends the design and assembly scope of organic solid materials.

With the developments of both the multicomponent materials and micro/nanostructures in mind, in this work, we have designed and developed the new type of organic solid-state materials by the assembly of 4,4′-dinitrostilbene-2,2′-disulfonate (DNS, Scheme 1A) anion with the guanidinium cation (GD, Scheme 1B). DNS is generally used as a fluorescent brightener in the chemical industry; moreover, the phenylenevinylene or stilbene unit in DNS has also attracted much interest because of its excellent optical and electronic

Received: June 29, 2013
Revised: August 8, 2013
Published: August 12, 2013

 © 2013 American Chemical Society dx.doi.org/10.1021/cg400979d | Cryst. Growth Des. 2013, 13, 4495−4503

Scheme 1. Chemical Structures of (A) 4,4′-Dinitrostilbene-2,2′-disulfonate (DNS) Anion and (B) Guanidinium Cation (GD)

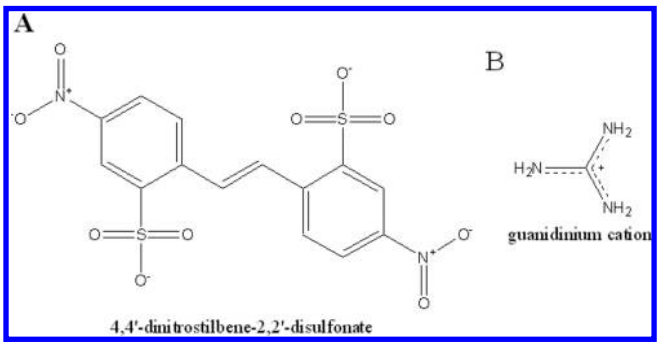

properties.[20] The selection of the guanidinium cation is based on the fact that it has been successfully served as a hydrogen-bonding coassembled motif with sulfonate-bearing anions for engineering bulk crystal topologies.[21] However, few guanidinium sulfonate systems have been observed in nanostructured crystals, and their exact properties at the micro/nanometer scale are still unknown. Compared with the pure sodium salt of DNS (Na_2DNS), the as-prepared GD_2DNS crystal at the micrometer size undergoes a red-shift emission as well as an enhanced fluorescence lifetime and photoluminescence quantum yield (PLQY). Periodic density functional theoretical (DFT) calculations further show that the difference in the cationic units can influence the frontier orbital distribution and electronic structure of DNS anions within the multicomponent crystals. Moreover, one-dimensional (1D) GD_2DNS nanobelts with high orientation can also be fabricated by a coprecipitation method under an ultrasound condition. The GD_2DNS nanobelts exhibit different photoresponse (emission wavelength and intensity) upon interaction with different nitroaromatic explosives. With a combination of experimental methodology and theoretical study on the micro/nanostructures, this work not only provides a feasible way to construct highly ordered micro/nanosized multicomponent organic solids but also gives a detailed understanding of the energy levels of the DNS-based materials. It is also expected that the GD_2DNS nanobelt system can potentially be applied in the field of luminescence sensors for explosives.

2. RESULTS AND DISCUSSION

A. Sodium Salt of DNS. The single crystal of Na_2DNS can be obtained by a single-step neutralization of H_2DNS and NaOH with a 1:2 ratio. The single crystal structure analysis shows that the Na_2DNS crystal features $P2_1/c$ symmetry. Figure 1a shows the typical side view of the Na_2DNS structure in the (100) direction, in which the adjacent NDS anions exhibit a staggered-type arrangement with the center distance of ca. 0.55 nm. The fluorescence spectra for the Na_2DNS sample were shown in Figure 1b. The excitation and emission positions are located at 441 and 485 nm, respectively. Moreover, the power-dependent emission spectrum of an individual crystal was measured for comparison with that of the bulk. Upon excitation by a laser at 405 nm, the Na_2DNS microcrystal showed enhanced fluorescent brightness with increasing excitation intensity, as shown in Figure 1c. Their emission intensities correlate nearly linearly with the excitation power (inset plot), illustrating that a one-phonon emission process is involved. The main emission peak of Na_2DNS appears at approximately 485 nm with the CIE 1931 color coordinates of (0.283, 0.458), illustrating that no obvious shift in the emission maximum of the individual crystal was observed compared to the Na_2DNS ensemble. The microcrystalline compositions with well-defined bluish green emission can be visible easily by the naked eye, as shown in the inset of Figure 1c.

B. GD_2DNS Single Crystal. By mixing an aqueous solution of Na_2DNS (0.005 mol) and an aqueous solution of GD (0.01 mol), the single crystal of GD_2DNS can readily be formed upon evaporation of the solvent. The crystal structure exhibited a layered structure with $P2_1/n$ symmetry, and the unit cell contains one crystalline water molecule. The DNS anions within the same layer present a parallel arrangement with the average distance between the neighboring DNS of 0.68 nm and the relative orientation of ca. 32.8°. Such arrangement fashion is favorable to the formation of the *J*-type aggregation within the crystals, and the presence of a layered stacking structure with a periodicity of 1.61 nm is related to the strong H-bonding assembly within the GD_2DNS. Different from the common GD-based assembled systems,[21] H-bonding modes in GD_2DNS consist of N−H···O═S and N−H···O═N between the GD and DNS units as well as N−H···O−H and S═O···H−O between the GD/DNS units and H_2O (Figure 2a). Figure 2b shows the excitation and emission spectra with the positions at 450 and 517 nm, respectively.

Figure 3 (panels a and b) show the microcrystalline GD_2DNS sample under optical and fluorescence microscopy, and the needlelike compositions can be visualized easily by the naked eye. A typical scanning electron microscopy (SEM) image of the GD_2DNS crystal ensemble is shown in Figure 3c. Further magnification shows that the crystal has a relatively smooth surface, and several defects can also be detected. The width of the crystals can be estimated to be ca. 10 μm, as shown

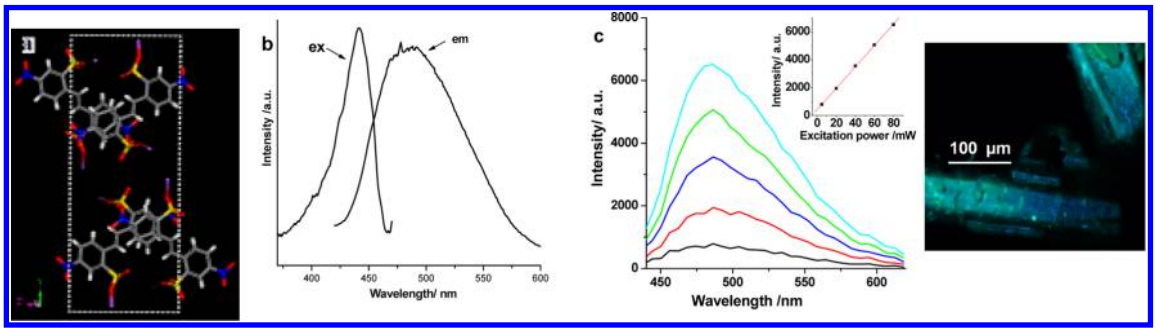

Figure 1. (a) Crystal structure [viewed from the (100) direction], (b) fluorescence spectra, and (c) power-dependent emission (inset shows the selected crystals under a fluorescence microscope) of Na_2DNS.

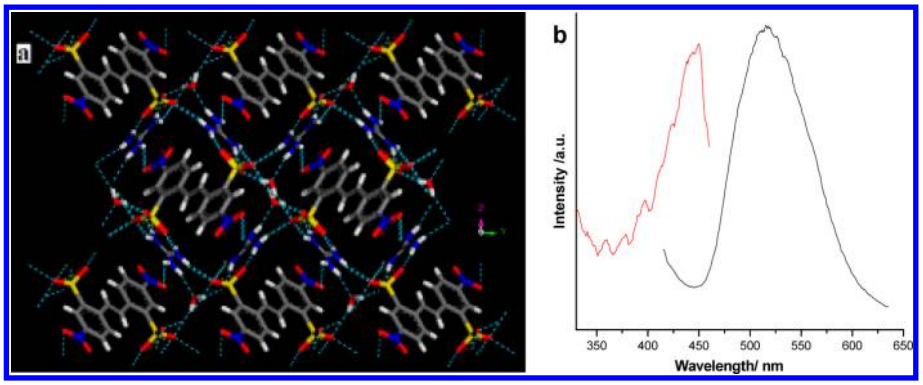

Figure 2. (a) Crystal structure [viewed from (100) direction] of GD_2DNS (the blue dash line is the H-bonding interaction) and (b) its fluorescence spectra.

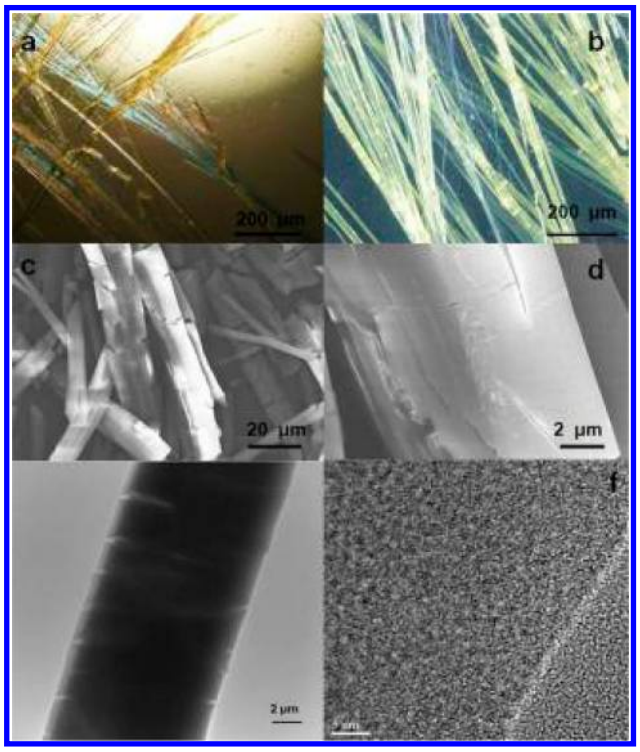

Figure 3. (a and b): GD_2DNS samples under optical and fluorescence microscopes; (c and d): SEM profiles for the GD_2DNS crystal at different magnifications; (e) TEM and (f) HRTEM images of a single GD_2DNS crystal.

in both SEM (Figure 3d) and transmission electron microscopy (TEM, Figure 3e) images. Figure 3f shows a typical high-resolution TEM (HRTEM) image of the edge of the crystal, in which the crystal plane is not well-solved, probably due to high thickness of the selected sample.

The power-dependent emission spectrum of a single GD_2DNS crystal was further measured and compared with that of the bulk. Upon laser excitation at 405 nm, the single crystal showed increasing fluorescence intensity with increasing excitation intensity, as shown in Figure 4. The main emission peak of the selected single crystal appeared at *ca.* 520 nm with the CIE 1931 color coordinates of (0.279, 0.653), and no obvious shift in the emission maximum of the individual crystal was observed compared to the ensemble. In addition, the typical dark-field image of the selected sample excited with laser

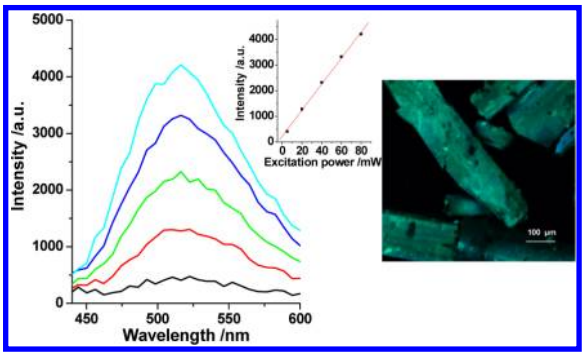

Figure 4. Power-dependent emission (inset shows the selected crystals under a fluorescence microscope) of Na_2DNS.

power of 80 mW is visible to the naked eye, as shown in the inset of Figure 4.

C. Comparison of Photophysical Properties of GD_2DNS and Na_2DNS. Compared with the microcrystalline Na_2DNS, the GD_2DNS single crystal undergoes a red-shift emission of ca. 32 nm. Moreover, the photoluminescence quantum yield (PLQY) enhanced from 0.37% (Na_2DNS) to 1.65% (GD_2DNS). In our opinion, the red shift can mainly be attributed to the fact that the arrangement fashion of the DNS anions transfer from the staggered form to the parallel stacking, as illustrated by the crystal structure analysis. As a result, the overlap of the electronic density of the DNS chromophore occurs. To further study the excited-state properties of the DNS-based crystal, the fluorescence lifetime of the samples was further recorded. The typical fluorescence decay curves of Na_2DNS and GD_2DNS are shown in Figure 5 and their corresponding fluorescence lifetimes were 0.34 and 0.70 ns, respectively. The enhancement of the fluorescence lifetimes is also in agreement with the latter structure favoring the formation of molecular excimers and *J*-type aggregations of DNS.

It was noted that the stilbene compound can be a two-photon emissive chromophore, and thus, two-photon excited fluorescence measurements were further made. Upon excitation by 800 nm of laser light, both the Na_2DNS (Figure 6a) and GD_2DNS (Figure 6b) crystals exhibit well-defined green-light photoemission with the position at 492 and 527 nm, respectively; the emission intensity shows a nearly quadratic increase as a function of the incident energy, confirming the two-photon absorption/emission mechanism of the DNS-based organic solids. Therefore, it can be concluded that the two-photon fluorescence can also be tuned by regulating the

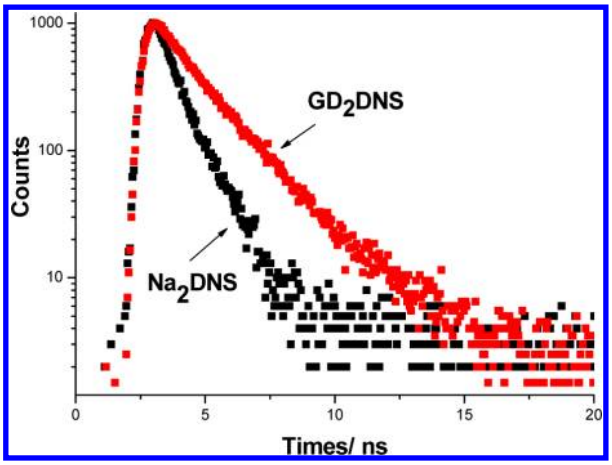

Figure 5. The fluorescence decay curves of the GD_2DNS and Na_2DNS.

arrangement fashion of DNS, and no obvious red- or blue shift of the two-photon fluorescence can be observed compared with those excited at 360 nm UV light, illustrating that the same emission process from one-photon and two-photon excited states to the ground state are involved.

D. Theoretical Calculations on the Na_2DNS and GD_2DNS. To better understand the energy level and electronic structure of the DNS-based multicomponent systems, periodic density functional theoretical (PDFT) calculations were performed on the Na_2DNS and GD_2DNS crystal models. For the Na_2DNS system, total electronic densities of states (TDOS) and partial electronic densities of states (PDOS) analyses (Figures S1 and S2 of the Supporting Information) show that the highest occupied molecular orbitals (HOMOs) are mainly populated on stilbene units and $-SO_3$ group in DNS as well as the Na atom, while the lowest unoccupied molecular orbitals (LUMOs) are solely located on 2p orbitals of the C atoms in DNS anions. This can be visualized by observing the frontier orbital profiles of Na_2DNS, as shown in Figure 7 (panels A and B), and such a result further indicates that the energy or electron transfer occurs between DNS and Na atom during the fluorescence process. For the GD_2DNS system, around the Fermi level, the TDOS mainly consisted of the 2p electrons of the C atoms in the DNS; both the HOMOs and LUMOs are contributed from the stilbene units and $-NO_2$ group (Figures S3 and S4 of the Supporting Information), suggesting that no obvious intramolecular and intermolecular energy transfer appears during the photoexcitation/emission process. These results show that the introduction of different cationic units can influence the frontier orbital distribution and electronic structure of DNS anions within the multicomponent crystals, which may further influence the luminescent properties of the organic solids, as shown in Experimental Section above.

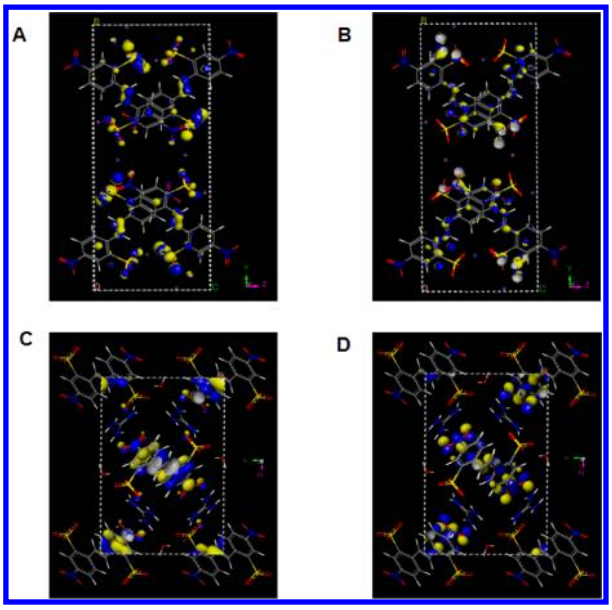

Figure 7. (A and C) HOMOs and (C and D) LUMOs profiles for Na_2DNS and GD_2DNS.

E. Fabrication of GD_2DNS Nanobelt. The GD and DNS with a 2:1 ratio were separately dissolved to obtain an aqueous solution and then simultaneously injected into a chloroform solution under ultrasound condition; the slurry sample was filtered or extended on a glass substrate. The powder XRD pattern of the obtained sample (Figure 8) is consistent well with the simulated XRD result from the GD_2DNS single crystals, further confirming that the multicomponent GD_2DNS sample can be obtained by the combined ultrasound and coprecipitation method. The synthesis of the GD_2DNS has taken advantage of the strong H-bonding recognition between the compositions. In addition, the strong (020) reflection

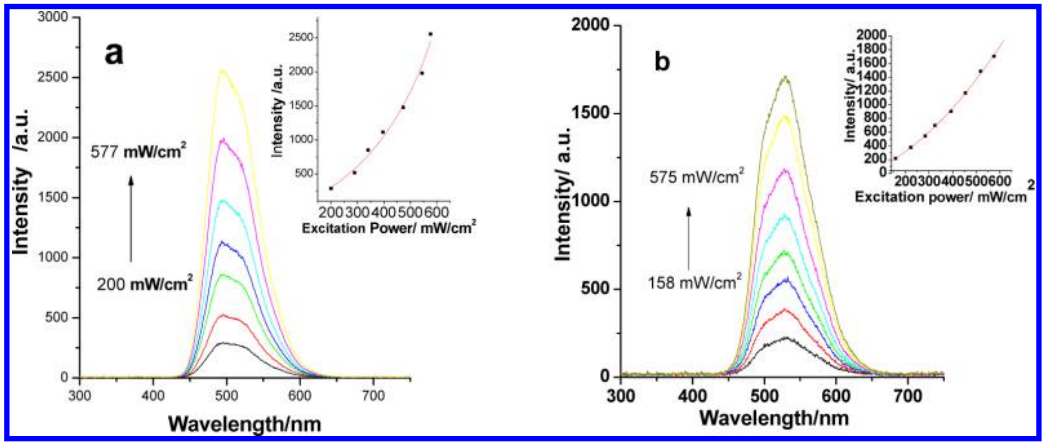

Figure 6. Two-photon fluorescence spectra of the (a) Na_2DNS and (b) GD_2DNS excited by an 800 nm laser under different pump intensities. Insets show the changes in intensity at 492 and 527 nm with increasing pump intensity.

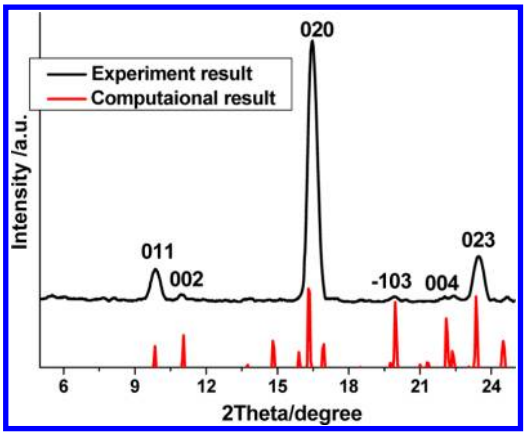

Figure 8. Experimental and simulated XRD results of the GD_2DNS sample.

accompanied by the absences of (002) and (004) reflections in the XRD profile can be observed, suggesting extremely good *b* axis oriented assembly of the as-prepared GD_2DNS sample. Figure 9a and 9b show the obtained sample under optical and fluorescence microscopes, from which it can be observed that the GD_2DNS exhibits one-dimensional (1D) beltlike morphology, which may be related to the 1D anisotropy of the DNS anions in the long-axis direction. The well-oriented nanostructures with high dispersion on the substrate can be obtained by diluting the as-prepared sample, as shown in Figure 9c. On the basis of the SEM observation, the products can be regarded as 1D nanobelts, and each individual nanostructure has a smooth surface and a uniform width of ca. 600 nm, as shown in Figure 9d. Figure 9e shows a typical TEM image of a single nanobelt, in which well-defined crystal planes with a lattice distance of ~1.6 nm can be further resolved along the long-axis direction of the nanobelt, as shown in the HRTEM image (Figure 9f), suggesting a high degree of molecular arrangement within the nanocrystal. Moreover, such observation is also in agreement with the preferred orientation in the (010) direction, as shown in the XRD pattern.

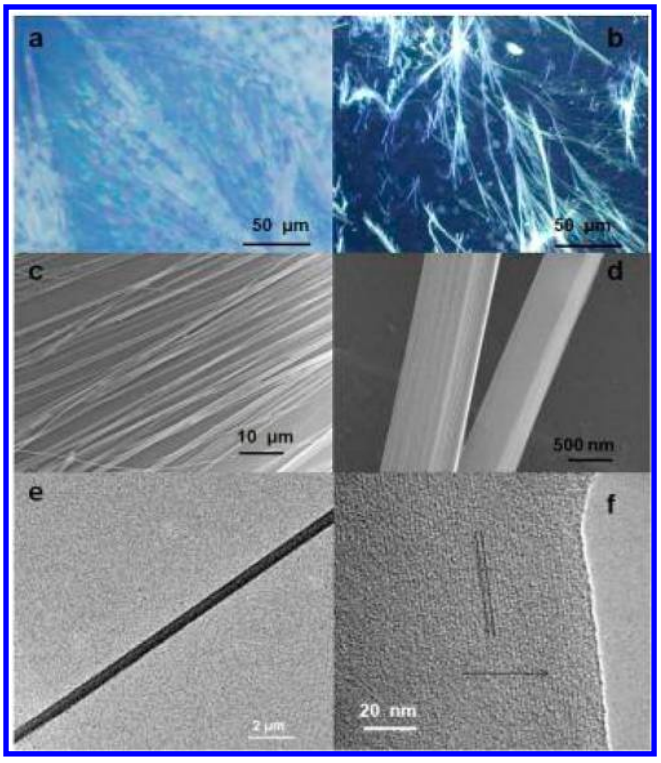

Figure 9. (a and b) GD_2DNS nanobelts under optical and fluorescence microscopes. (c and d) SEM profiles for the GD_2DNS sample on a glass substrate at different magnifications. (e) TEM and (f) HRTEM images of a single GD_2DNS nanobelt.

The photophysical properties of the as-prepared GD_2DNS nanobelts were further detected to obtain the insight into the size-dependent effect of the multicomponent GD_2DNS system. The typical fluorescence spectra are shown in Figure 10a, and the excitation and emission position appear at 452 and 496 nm, respectively. Compared with the GD_2DNS crystal at the micrometer level, a blue-shift of ca. 24 nm occurs for the nanobelt samples; such behavior may be related to the fact that the decrease of the size results in lattice softening and weaker interaction energies, and thus the band gap was further increased.[16] The analysis of the fluorescence decays (Figure 10b) reveals that the fluorescence lifetime of the nanobelt samples is prolonged to 0.85 ns, as compared to the microdimensional crystals (0.70 ns). This increase may be attributed to the deaggregation of the crystals, which decrease the excited-state nonradioactive relaxation from excitonic coupling between the crystal particles. To the best of our knowledge, although the size-dependent optical properties have largely been reported in both inorganic and pure organic nanomaterial systems,[22] very few studies have focused on such multicomponent organic nanobelts. In addition, power-dependent excitation on the GD_2DNS nanobelts under 405 and 800 nm laser was further measured; it can be observed that the nanobelt sample exhibits both one-photon (Figure 11a) and two-photon (Figure 11b) emission with the emission peak of ca. 500 nm, which is close to that of the nanobelt ensemble.

F. Reversible Photoresponse of GD_2DNS Nanobelt to Nitroaromatic Explosive Compounds. Recently, the organic fluorescence-based sensor for the detection of explosives has drawn much attention due to the high sensitivity.[23] In this work, it was noted that the GD_2DNS nanobelt features a highly exposed surface, which can contact with the analytes effectively. Herein, the ability of the GD_2DNS nanobelt to detect nitroaromatic explosives [trinitrotoluene (TNT), picric acid (PA) and *m*-dinitrobenzen (mDNB)] was studied by adding small amount of explosives in methanol solution with 1, 5, 10, and 20 ppm into the GD_2DNS nanobelt samples. Figure 12A shows the typical emission spectra of the GD_2DNS nanobelt responding to the TNT sample. It can be observed that the fluorescent position undergoes a red shift toward 536 nm upon interaction with TNT, and the photoemission intensity of the GD_2DNS nanobelt decreases systematically upon increasing the TNT concentration. Similar behavior can also be observed when detecting the PA and mDNB explosives, in which the emissive wavelengths of the GD_2DNS nanobelt moved to 520 and 511 nm, respectively (Figure 12B and 12C). Moreover, the recovery and reproducibility of the fluorescence for the GD_2DNS nanobelt were further investigated. After the nanobelt was eluted with methanol and then heated for full removal of the explosives, the fluorescence wavelength and intensity can nearly recover to their initial state. Figure 13 shows the typical examples of the variation of the luminescence dependent on the alternate treated with 1 ppm TNT and methanol over four continuous cycles, which shows that the wavelength and the intensity ratio

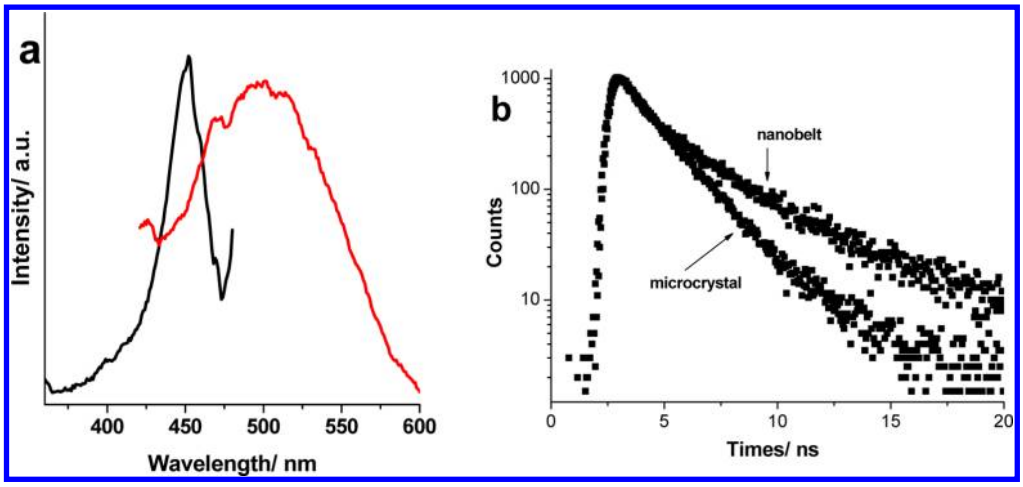

Figure 10. (a) Fluorescence spectra and (b) fluorescence decay profile of the GD_2DNS nanobelts and microcrystal.

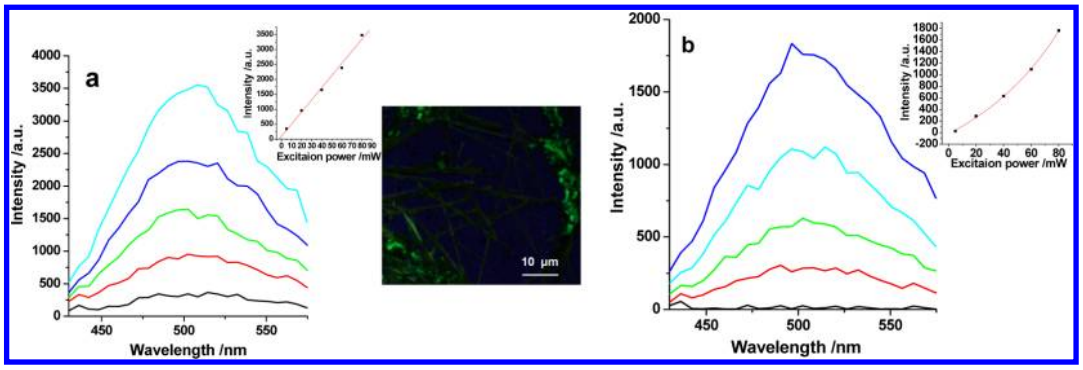

Figure 11. Power-dependent emission (inset shows the selected crystals under a fluorescence microscope) of the GD_2DNS nanobelt excited at (a) 405 and (b) 800 nm.

between two states can readily be cycled, confirming the recovered nanobelt could also be reused immediately.

To date, most reported fluorescent sensors[24] for detecting explosives are based on the fluorescence quenching mechanism as a result of interaction between chromophore materials and analytes; their fluorescence emissive position has nearly no change, and such intensity-based detection may be largely influenced by the stability of the excitation light source. For this GD_2DNS nanobelt system, it can be observed that the fluorescence wavelength can vary dependent on three different nitroaromatic explosives, which facilitates the detection for the analytes. From a molecular recognition perspective, the electron-withdrawing unit ($-NO_2$ group) in nitroaromatic compounds can potentially form a hydrogen-bond interaction with the GD cation in the GD_2DNS nanobelt, which may further influence the electronic structure of the DNS anions within the GD_2DNS nanobelt and thus alter the emission behaviors of the nanobelt. The remarkable change in the luminescence and the reversibility guarantee that the as-prepared nanobelt can potentially be used as an explosive-induced luminescence sensor.

3. CONCLUSION

In summary, well-organized dinitrostilbene-based multicomponent organic crystals with tunable micro/nanostructures have been fabricated. The as-prepared GD_2DNS bulk crystal exhibits a 2D pillared structure with the chromophores parallel with each other and shows a red-shift emission as well as enhanced PLQY and fluorescence lifetime compared with the Na_2DNS sample, suggesting that the alternation of the fluorescence properties can be achieved by modulating the arrangement fashion of the DNS anions within the crystal. Furthermore, the GD_2DNS nanobelt with well-aligned orientation can be further obtained by a combined ultrasound and coprecipitation method. The fluorescence of the GD_2DNS nanobelt undergoes a blue shift compared with its bulk crystal, suggesting the luminescent properties of the multicomponent system can also be modified by adjusting the micro/nanometer size. Moreover, the GD_2DNS nanobelts exhibit a reversible photoresponse (such as wavelength and intensity) upon treatment with different nitroaromatic explosives, indicating that the as-prepared nanobelt can be potentially used as a luminescence detector for explosives. It is expected that the strategy to form micro/nanocrystal with tunable components and morphologies can be extended to other chromophore systems for developing new types of organic luminescent materials and sensors. Further work is still underway with the research on the gas phase detection of nitroaromatic compounds.

4. EXPERIMENTAL SECTION

4.1. Reagents. 4,4′-Dinitrostilbene-2,2′-disulphonic acid (H_2DNS) and guanidinium chloride (GD), NaOH, and chloroform were purchased from Sigma Chemical Company Ltd. and used without further purification.

4.2. Synthesis of Sodium Salt of DNS and Microsized GD_2DNS. A 100 mL aqueous solution containing H_2DNS (0.01 mol) and NaOH (0.02 mol) was slowly evaporated, and the single crystal of

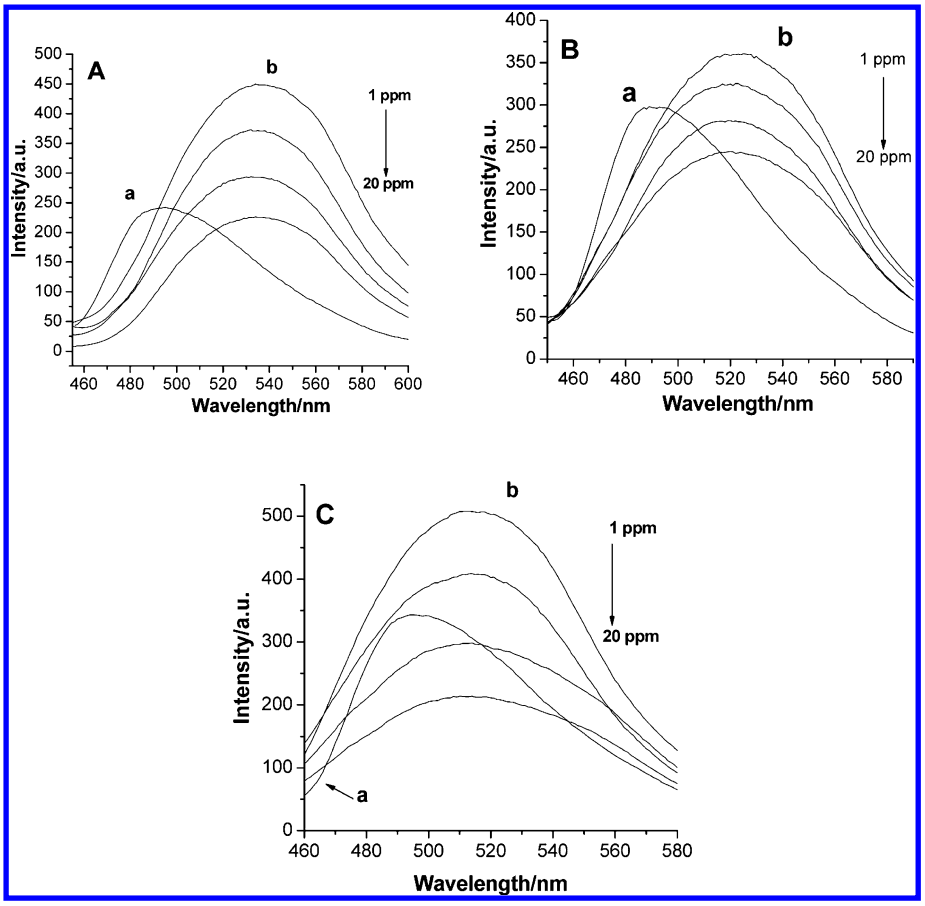

Figure 12. GD_2DNS nanobelts (a) before and (b) after treatment with different concentrations (1, 5, 10, and 20 ppm) of (A) TNT, (B) PA, and (C) mDNB.

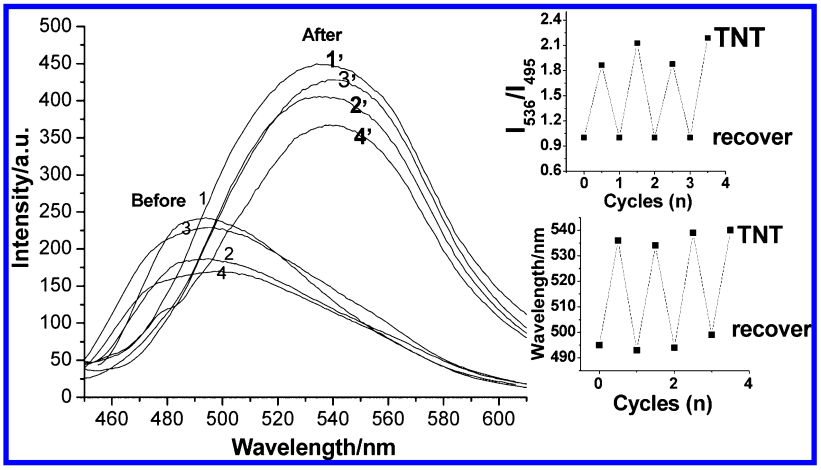

Figure 13. The fluorescent spectra of the GD_2DNS nanobelt after alternate treatment by TNT (1 ppm) and methanol over four continuous reversible cycles [the insets show the fluorescent wavelength and the intensity ratio between the maximum wavelengths (495 and 536 nm) of two states].

Na_2DNS was formed within two weeks. Single crystals of GD_2DNS were obtained by mixing a 50 mL aqueous solution of Na_2DNS (0.005 mol) and a 50 mL aqueous solution of GD (0.01 mol) and were allowed to evaporate within one day. Thermogravimetry analysis (TGA, Figure S5 of the Supporting Information) shows that the dehydration occurs for both the samples before 150 °C and the amount of water in the samples can be estimated as 18.6% and 6.4%, which is close to the results based on single crystal analysis (19.4% and 6.2%). Elemental analysis gave C, 28.8%; H, 3.5%; N, 4.8%; S, 11.0% and C, 33.1%; H, 4.1%; N, 19.2%; S, 10.9% for the Na_2DNS and GD_2DNS samples, respectively. Therefore, the chemical compositions of two samples can be determined as $C_{14}H_8N_2S_2O_{10}Na_2(6H_2O)$ and $(CN_3H_6)_{1.96}(C_{14}H_8N_2O_{10}S_2)(2H_2O)$.

4.3. Fabrication of GD_2DNS Nanobelts. The nanobelts were obtained by a combined ultrasound and coprecipitation method. In a typical process, 100 mL of an aqueous solution containing 0.002 mol of GD and 100 mL of an aqueous solution containing 0.001 mol of DNS were simultaneously added to 50 mL of a chloroform solution under low-intensity ultrasonic radiation (using an ultrasonic cleaning bath with a frequency of 25 kHz) and mixed for 3 min. The resulting

slurry was extended on a glass or quartz substrate and allowed to dry naturally under ambient conditions.

4.4. Periodic Density Functional Theoretical (PDFT) Calculation. PDFT method was performed using the Dmol3[25] module in Material Studio.[26] The single crystal structures of Na_2DNS and GD_2DNS were selected as the initial models, which were optimized by the Perdew–Wang (PW91)[27] generalized gradient approximation (GGA) method with the double numerical basis sets plus the polarization function (DNP). The SCF convergence criterion was within 1.0×10^{-5} hartree/atom, and the convergence criterion of structure optimization was 1.0×10^{-3} hartree/bohr. The Brillouin zone (BZ) was sampled by $1 \times 1 \times 1$ k points, and test calculations revealed that an increased number of k points does not influence the results.

4.5. Characterization. The powder X-ray diffraction patterns were recorded on a X-Pert PRO MPD powder X-ray diffractometer, using Cu Kα radiation (0.154184 nm) at 30 kV, 40 mA with a scanning rate of 10°/min, and a 2θ angle ranging from 3 to 50°. Single crystal X-ray diffraction data were collected on a Nonius KappaCCD diffractometer equipped with a graphite monochromator and an Oxford cryostream, using Mo Kα radiation. Thermogravimetry was measured on a PCT-1A thermal analysis system under ambient atmosphere with a heating rate of 10 °C/min. Carbon, hydrogen, nitrogen, and sulfur analyses were carried out using a Perkin-Elmer Elementarvario elemental analysis instrument. The solid-state fluorescence spectra were recorded on a RF-5301PC fluorospectrophotometer with 360 nm excitation light. The width of both the excitation and emission slit was 3 nm. PLQY and 1931 CIE color coordinates were measured using an HORIBA Jobin Yvon FluoroMax-4 spectrofluorometer, equipped with an F-3018 integrating sphere. Two-photon fluorescence of the samples was excited by a 800 nm laser on a Tsunami-Spitfire-OPA-800C ultrafast optical parameter amplifier (Spectra-Physics). The fluorescence images were obtained on an Olympus U-RFLT50 fluorescence microscope. The morphology of samples was investigated using a scanning electron microscope (SEM Hitachi S-3500) equipped with an energy-dispersive X-ray analysis (EDX) attachment, and the accelerating voltage applied was 20 kV.

■ ASSOCIATED CONTENT

Supporting Information

Total and partial electronic density of states (e.g., TDOS and PDOS) profiles for Na_2DNS (Figure S1); TDOS and PDOS profiles for different atoms in Na_2DNS (Figure S2); TDOS and PDOS profiles for GD_2DNS (Figure S3); TDOS and PDOS profiles for different atoms in GD_2DNS (Figure S4); Thermogravimetry analysis of the (a) Na_2DNS and (b) GD_2DNS samples (Figure S5). This material is available free of charge via the Internet at http://pubs.acs.org.

■ AUTHOR INFORMATION

Corresponding Author

*E-mail: yandongpeng001@163.com and yandp@mail.buct.edu.cn. Fax: +86-10-64425385. Tel: +86-10-64412131.

Notes

The authors declare no competing financial interest.

■ ACKNOWLEDGMENTS

This work was supported by the National Basic Research Program of China (Grant 2014CB932103), the National Natural Science Foundation of China, and the 111 Project (Grant B07004), Central University Research Funds, and Program for Changjiang Scholars, and the Innovative Research Team in University (PCSIRT: IRT1205).

■ REFERENCES

(1) (a) Bosshard, C.; Wong, M. S.; Gunter, P. *Adv. Mater.* **1997**, *9*, 837. (b) Langhals, H.; Krotz, O.; Polborn, K.; Mayer, P. *Angew. Chem., Int. Ed.* **2005**, *44*, 2427. (c) Zhao, C.-H.; Wakamiya, A.; Inukai, Y.; Yamaguchi, S. *J. Am. Chem. Soc.* **2006**, *128*, 15934. (d) Xie, Z.; Wang, H.; Li, F.; Xie, W.; Liu, L.; Yang, B.; Ye, L.; Ma, Y. *Cryst. Growth. Des.* **2007**, *7*, 2512. (e) He, F.; Tian, L. L.; Tian, X. Y.; Xu, H.; Wang, Y. H.; Xie, W. J.; Hanif, M.; Xia, J. L.; Shen, F. Z.; Yang, B.; Li, F.; Ma, Y. G.; Yang, Y. Q.; Shen, J. C. *Adv. Funct. Mater.* **2007**, *17*, 1551.

(2) (a) Ning, Z.; Chen, Z.; Zhang, Q.; Yan, Y.; Qian, S.; Cao, Y.; Tian, H. *Adv. Funct. Mater.* **2007**, *17*, 3799. (b) Yan, D. P.; Lu, J.; Wei, M.; Han, J. B.; Ma, J.; Li, F.; Evans, D. G.; Duan, X. *Angew. Chem., Int. Ed.* **2009**, *48*, 3073. (c) Strassert, C. A.; Chien, C.-H.; Lopez, M. D. G.; Kourkoulos, D.; Hertel, D.; Meerholz, K.; De Cola, L. *Angew. Chem., Int. Ed.* **2011**, *50*, 946. (d) Hellerich, E. S.; Intemann, J. J.; Cai, M.; Liu, R.; Ewan, M. D.; Tlach, B. C.; Jeffries-EL, M.; Shinar, R.; Shinar, J. *J. Mater. Chem. C* **2013**, *1*, 5191. (e) Sun, D.; Fu, Q.; Ren, Z.; Li, W.; Li, H.; Ma, D.; Yan, S. *J. Mater. Chem. C* **2013**, *1*, 5344. (f) Kim, Y. H.; Lee, J.; Hofmann, S.; Gather, M. C.; Müller-Meskamp, L.; Leo, K. *Adv. Funct. Mater.* **2013**, *23*, 3763.

(3) (a) An, B.-K.; Gihm, S. H.; Chung, J. W.; Park, C. R.; Kwon, S.-K.; Park, S. Y. *J. Am. Chem. Soc.* **2009**, *131*, 3950. (b) Zhang, X.; Rehm, S.; Safont-Sempere, M. M.; Würthner, F. *Nat. Chem.* **2009**, *1*, 623. (c) Li, C.; Zhang, Y.; Hu, J.; Cheng, J.; Liu, S. *Angew. Chem., Int. Ed.* **2010**, *49*, 5120. (d) Yan, D. P.; Lu, J.; Ma, J.; Qin, S.; Wei, M.; Evans, D. G.; Duan, X. *Angew. Chem., Int. Ed.* **2011**, *50*, 7037. (e) Feng, J.; Tian, K.; Hu, D.; Wang, S.; Li, S.; Zeng, Y.; Li, Y.; Yang, G. *Angew. Chem., Int. Ed.* **2011**, *50*, 8072. (f) Shi, H.; Sun, H.; Yang, H.; Liu, S.; Jenkins, G.; Feng, W.; Li, F.; Zhao, Q.; Liu, B.; Huang, W. *Adv. Funct. Mater.* **2013**, *23*, 3268.

(4) (a) Irie, M.; Fukaminato, T.; Sasaki, T.; Tamai, N.; Kawai, T. *Nature* **2002**, *420*, 759. (b) Zhang, G.; Lu, J.; Sabat, M.; Fraser, C. L. *J. Am. Chem. Soc.* **2010**, *132*, 2160. (c) Sagara, Y.; Kato, T. *Angew. Chem., Int. Ed.* **2011**, *50*, 9128. (d) Sagara, Y.; Kato, T. *Angew. Chem., Int. Ed.* **2011**, *50*, 9128. (e) Sagara, Y.; Kato, T. *Nat. Chem.* **2009**, *1*, 605. (f) Gu, X.; Yao, J.; Zhang, G.; Yan, Y.; Zhang, C.; Peng, Q.; Liao, Q.; Wu, Y.; Xu, Z.; Zhao, Y. S.; Fu, H.; Zhang, D. *Adv. Funct. Mater.* **2012**, *22*, 4862.

(5) (a) Mutai, T.; Satou, H.; Araki, K. *Nat. Mater.* **2005**, *4*, 685. (b) Collas, A.; De Borger, R.; Amanova, T.; Blockhuys, F. *CrystEngComm* **2011**, *13*, 702.

(6) Kunzelman, J.; Kinami, M.; Crenshaw, B. R.; Protasiewicz, J. D.; Weder, C. *Adv. Mater.* **2008**, *20*, 119.

(7) (a) Mutai, T.; Tomoda, H.; Ohkawa, T.; Yabe, Y.; Araki, K. *Angew. Chem., Int. Ed.* **2008**, *47*, 9522. (b) Yan, D. P.; Evans, D. G. *Mater. Horiz.* **2013**, DOI: 10.1039/C3MH00023K.

(8) (a) Lee, T.; Wang, P. Y. *Cryst. Growth Des.* **2010**, *10*, 1419. (b) Yan, D. P.; Yang, H.; Meng, Q.; Lin, H.; Wei, M. *Adv. Funct. Mater.* **2013**, DOI: 10.1002/adfm.201302072.

(9) (a) Shen, Q.; Wei, H.; Zou, W.; Sun, H.; Jin, W. *CrystEngComm* **2012**, *14*, 1010. (b) Papaefstathiou, G. S.; Zhong, Z.; Geng, L.; MacGillivray, L. R. *J. Am. Chem. Soc.* **2004**, *126*, 9158. (c) Landenberger, K. B.; Bolton, O. J.; Matzger, A. J. *Angew. Chem., Int. Ed.* **2013**, *52*, 6468.

(10) (a) Anthony, S. P.; Varughese, S.; Draper, S. M. *Chem. Commun.* **2009**, 7500. (b) Yan, D.; Delori, A.; Lloyd, G. O.; Patel, B.; Friščić, T.; Day, G. M.; Bučar, D.-K; Jones, W.; Lu, J.; Wei, M.; Evans, D. G.; Duan, X. *CrystEngComm* **2012**, *14*, 5121. (c) Yan, D.; Patel, B.; Delori, A.; Jones, W.; Duan, X. *Cryst. Growth Des.* **2013**, *13*, 333.

(11) (a) Yan, D.; Delori, A.; Lloyd, G. O.; Friščić, T.; Day, G. M.; Jones, W.; Lu, J.; Wei, M.; Evans, D. G.; Duan, X. *Angew. Chem., Int. Ed.* **2011**, *50*, 12483. (b) Yan, D.; Bučar, D. K.; Delori, A.; Patel, B.; Lloyd, G. O.; Jones, W.; Duan, X. *Chem.—Eur. J.* **2013**, *19*, 8213.

(12) (a) Wuest, D. J. *Nat. Chem.* **2012**, *4*, 74. (b) Meazzal, L.; Foster, J. A.; Fucke, K.; Metrangolol, P.; Resnati1, G.; Steed, J. W. *Nat. Chem.* **2013**, *5*, 42.

(13) (a) Desiraju, G. R. *Angew. Chem., Int. Ed.* **1995**, *34*, 2311. (b) Desiraju, G. R. *Acc. Chem. Res.* **1996**, *29*, 441. (c) Nangia, A. *Acc. Chem. Res.* **2008**, *41*, 595. (d) Cavallo, G.; Aakeröy, C. B.; Champness,

N. R.; Janiak, C. *CrystEngComm* **2010**, *12*, 22. (e) Nishiguchi, N.; Sato, T.; Kinuta, T.; Kuroda, R.; Matsubara, Y.; Imai, Y. *Cryst. Growth Des.* **2011**, *11*, 827. (f) Mizobe, Y.; Tohnai, N.; Miyata, M.; Hasegawa, Y. *Chem. Commun.* **2005**, 1839. (g) Metrangolo, P.; Neukirch, H.; Pilati, T.; Resnati, G. *Acc. Chem. Res.* **2005**, *38*, 386. (h) Landenberger, K. B.; Matzger, A. J. *Cryst. Growth Des.* **2012**, *12*, 3603. (i) Jun, Y.-S.; Lee, E. Z.; Wang, X.; Hong, W. H.; Stucky, G. D.; Thomas, A. *Adv. Funct. Mater.* **2013**, *23*, 3661.

(14) (a) Hou, G. G.; Ma, J. P.; Wang, L.; Wang, P.; Dong, Y. B.; Huang, R. Q. *CrystEngComm* **2010**, *12*, 4287. (b) Li, J.; Takaishi, S.; Fujinuma, N.; Endo, K.; Yamashita, M.; Matsuzaki, H.; Okamoto, H.; Sawabe, K.; Takenobu, T.; Iwasa, Y. *J. Mater. Chem.* **2011**, *21*, 17662. (c) Luo, J.; Li, L.; Song, Y.; Pei, J. *Chem.—Eur. J.* **2011**, *17*, 10515.

(15) For examples: (a) Simonsen, A. C.; Rubahn, H.-G. *Nano Lett.* **2002**, *2*, 1379. (b) Zhang, X.; Zhang, X.; Zou, K.; Lee, C.-S.; Lee, S.-T. *J. Am. Chem. Soc.* **2007**, *129*, 3527. (c) Sun, Y.; Ye, K.; Zhang, H.; Zhang, J.; Zhao, L.; Li, B.; Yang, G.; Yang, B.; Wang, Y.; Lai, S.-W.; Che, C.-M. *Angew. Chem., Int. Ed.* **2006**, *45*, 1825. (d) Herrikhuyzen, J. V.; George, S. J.; Vos, M. R. J.; Sommerdijk, N. A. J. M.; Ajayaghosh, A.; Meskers, S. C. J.; Schenning, A. P. H. J. *Angew. Chem., Int. Ed.* **2007**, *46*, 1825. (e) Anthony, S. P.; Draper, S. M. *J. Phys. Chem. C* **2010**, *114*, 11708.

(16) Liao, Q.; Fu, H.; Wang, C.; Yao, J. *Angew. Chem., Int. Ed.* **2011**, *50*, 4942.

(17) (a) Naddo, T.; Che, Y.; Zhang, W.; Balakrishnan, K. X. Y.; Yen, M.; Zhao, J.; Moore, J. S.; Zang, L. *J. Am. Chem. Soc.* **2007**, *129*, 6978. (b) Ajayaghosh, A.; Praveen, V. K. *Acc. Chem. Res.* **2007**, *40*, 644.

(18) (a) Luo, J.; Lei, T.; Wang, L.; Ma, Y.; Cao, Y.; Wang, J.; Pei, J. *J. Am. Chem. Soc.* **2009**, *131*, 2076. (b) Yan, D.; Jones, W.; Fan, G.; Wei, M.; Evans, D. G. *J. Mater. Chem. C* **2013**, *1*, 4138.

(19) (a) Takahashi, S.; Miura, S. H.; Kasai, H.; Okada, S.; Oikawa, H.; Nakanishi, H. *J. Am. Chem. Soc.* **2002**, *124*, 10944. (b) Karunatilaka, C.; Bučar, D. K.; Ditzler, L. R.; Friščić, T.; Swenson, D. C.; MacGillivray, L. R.; Tivanski, A. V. *Angew. Chem., Int. Ed.* **2011**, *50*, 8642. (c) Sander, J. R. G.; Bučar, D. K.; Henry, R. F.; Zhang, G. G. Z.; MacGillivray, L. R. *Angew. Chem., Int. Ed.* **2010**, *49*, 7284.

(20) (a) Hong, Y.; Lam, J. W. Y.; Tang, B. Z. *Chem. Commun.* **2009**, 4332. (b) An, B. K.; Gierschner, J.; Park, S. Y. *Acc. Chem. Res.* **2012**, *45*, 544. (c) Zhu, L.; Ma, X.; Ji, F.; Wang, Q.; Tian, H. *Chem.—Eur. J.* **2007**, *13*, 9216. (d) Fu, W.; Kosmidis, C.; Schmid, W. E.; Trushin, S. A. *Angew. Chem., Int. Ed.* **2004**, *43*, 4178. (e) Zhu, L.; Yan, H.; Nguyen, K. T.; Tian, H.; Zhao, Y. *Chem. Commun.* **2012**, *48*, 4290. (f) Yan, D. P.; Lu, J.; Ma, J.; Wei, M.; Evans, D. G.; Duan, X. *Angew. Chem., Int. Ed.* **2011**, *50*, 720.

(21) (a) Holman, K. T.; Pivovar, A. M.; Ward, M. D. *Science* **2001**, *294*, 1907. (b) Abrahams, B. F.; Haywood, M. G.; Robson, R. *CrystEngComm* **2005**, *7*, 629.

(22) (a) Peng, X.; Manna, L.; Yang, W.; Wickham, J.; Scher, E.; Kadavanich, A.; Alivisatos, A. P. *Nature* **2000**, *404*, 59. (b) Yu, W. W.; Qu, L.; Guo, W.; Peng, X. *Chem. Mater.* **2003**, *15*, 2854. (c) Zhao, Y. S.; Fu, H.; Peng, A.; Ma, Y.; Xiao, D.; Yao, J. *Adv. Mater.* **2008**, *20*, 2859.

(23) (a) Liu, Y.; Mills, R. C.; Boncella, J. M.; Schanze, K. S. *Langmuir* **2001**, *17*, 7452. (b) Xiang, Z.; Cao, D. *Macromol. Rapid Commun.* **2012**, *33*, 1184. (c) Magde, T. S. J. D.; Trogler, W. C. *Chem. Commun.* **2005**, 5465. (d) Thomas, S. W., III; Joly, G. D.; Swager, T. M. *Chem. Rev.* **2007**, *107*, 1339. (e) Ma, H.; Gao, R.; Yan, D.; Zhao, J.; Wei, M. *J. Mater. Chem. C* **2013**, *1*, 4128.

(24) (a) Hu, X. M.; Chen, Q.; Zhou, D.; Cao, J.; He, Y.-J.; Han, B.-H. *Polym. Chem.* **2011**, *2*, 1124. (b) Shi, L.; He, C.; Zhu, D.; He, Q.; Li, Y.; Chen, Y.; Sun, Y.; Fu, Y.; Wen, D.; Cao, H.; Cheng, J. *J. Mater. Chem.* **2012**, *22*, 11629.

(25) Delley, B. J. *Chem. Phys.* **2000**, *113*, 7756.

(26) *Dmol3Module, MS Modeling*, version 2.2; Accelrys Inc.: San, Diego, CA, 2003.

(27) Perdew, J. P.; Chevary, J. A.; Vosko, S. H.; Jackson, K. A.; Pederson, M. R.; Singh, D. J.; Fiolhais, C. *Phys. Rev. B* **1992**, *46*, 6671.